GIGYF1/2-Driven Cooperation between ZNF598 and TTP in Posttranscriptional Regulation of Inflammatory Signaling

Tollenaere, Maxim A X; Tiedje, Christopher; Rasmussen, Simon; Nielsen, Julie C; Vind, Anna C; Blasius, Melanie; Batth, Tanveer S; Mailand, Niels; Olsen, Jesper V; Gaestel, Matthias; Bekker-Jensen, Simon

Published in:
Cell Reports

DOI:
10.1016/j.celrep.2019.03.006

Publication date:
2019

Document version
Publisher's PDF, also known as Version of record

Cell Reports

GIGYF1/2-Driven Cooperation between ZNF598 and TTP in Posttranscriptional Regulation of Inflammatory Signaling

Graphical Abstract

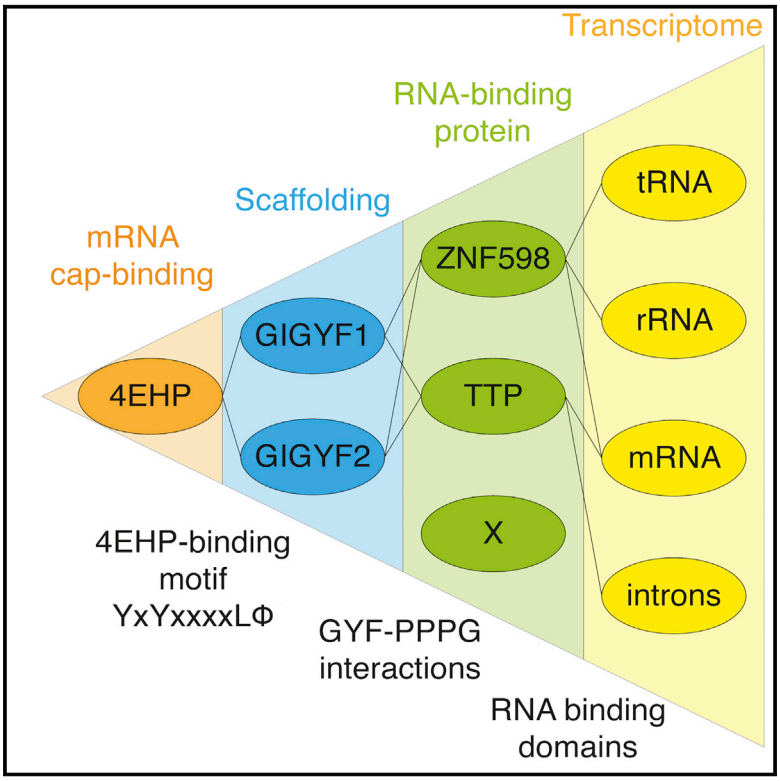

Highlights

- Proline stretches in ZNF598 are bound by the GYF domain of GIGYF1 and GIGYF2
- GIGYF1/2 interaction integrates ZNF598 into a complex that represses mRNA translation
- ZNF598 binds to and regulates the abundance of inflammation-associated mRNA transcripts
- The mRNA-binding repertoire of ZNF598 partially overlaps that of TTP/ZFP36

Authors

Maxim A.X. Tollenaere, Christopher Tiedje, Simon Rasmussen, ..., Jesper V. Olsen, Matthias Gaestel, Simon Bekker-Jensen

Correspondence

sbj@sund.ku.dk

In Brief

Tollenaere et al. highlight a structural and functional resemblance between the ribosome-associated ubiquitin ligase ZNF598 and TTP, the negative regulator of inflammation-associated mRNA stability. Like TTP, ZNF598 contains proline stretches that are bound by GYF domain-containing proteins, binds cytokine mRNAs, and represses inflammatory signaling in resting cells.

Tollenaere et al., 2019, Cell Reports *26*, 3511–3521
March 26, 2019
https://doi.org/10.1016/j.celrep.2019.03.006

CellPress

Cell Reports
Report

GIGYF1/2-Driven Cooperation between ZNF598 and TTP in Posttranscriptional Regulation of Inflammatory Signaling

Maxim A.X. Tollenaere,[1,6,7] Christopher Tiedje,[1,6] Simon Rasmussen,[2] Julie C. Nielsen,[1] Anna C. Vind,[1] Melanie Blasius,[1] Tanveer S. Batth,[3] Niels Mailand,[4] Jesper V. Olsen,[3] Matthias Gaestel,[5] and Simon Bekker-Jensen[1,8,*]

[1]Department of Cellular and Molecular Medicine, Center for Healthy Aging, University of Copenhagen, Blegdamsvej 3B, 2200 Copenhagen, Denmark

[2]Department of Plant and Environmental Sciences, Copenhagen Plant Science Centre, University of Copenhagen, 1871 Frederiksberg, Denmark

[3]Mass Spectrometry for Quantitative Proteomics, Proteomics Program, The Novo Nordisk Foundation Center for Protein Research, Faculty of Health and Medical Sciences, University of Copenhagen, Blegdamsvej 3B, 2200 Copenhagen, Denmark

[4]Ubiquitin Signaling Group, Protein Signaling Program, The Novo Nordisk Foundation Center for Protein Research, Faculty of Health and Medical Sciences, University of Copenhagen, Blegdamsvej 3B, 2200 Copenhagen, Denmark

[5]Institute of Cell Biochemistry, Hannover Medical School (MHH), 30625 Hannover, Germany

[6]These authors contributed equally

[7]Present address: LEO Pharma A/S, Industriparken 55, 2750 Ballerup, Denmark

[8]Lead Contact

*Correspondence: sbj@sund.ku.dk

https://doi.org/10.1016/j.celrep.2019.03.006

SUMMARY

Inflammatory signaling is restricted through degradation and the translational repression of cytokine mRNAs. A key factor in this regulation is tristetraprolin (TTP), an RNA-binding protein (RBP) that recruits RNA-destabilizing factors and the translation inhibitory complex 4EHP-GIGYF1/2 to AU-rich element (ARE)-containing mRNAs. Here, we show that the RBP ZNF598 contributes to the same regulatory module in a TTP-like manner. Similar to TTP, ZNF598 harbors three proline-rich motifs that bind the GYF domain of GIGYF1. RNA sequencing experiments showed that ZNF598 is required for the regulation of known TTP targets, including IL-8 and CSF2 mRNA. Furthermore, we demonstrate that ZNF598 binds to IL-8 mRNA, but not TNF mRNA. Collectively, our findings highlight that ZNF598 functions as an RBP that buffers the level of a range of mRNAs. We propose that ZNF598 is a TTP-like factor that can contribute to the regulation of the inflammatory potential of cytokine-producing cells.

INTRODUCTION

Multi-layered posttranscriptional regulation of gene expression allows for rapid cellular transitions and adaptation to diverse stimuli (Gerstberger et al., 2014). The production of cytokines and other inflammatory mediators by immune cells is regulated through these mechanisms, a key example being the destabilizing effect on cytokine transcripts exerted by the RNA-binding protein tristetraprolin (TTP/ZFP36/TIS11) (Clark and Dean, 2016; Tiedje et al., 2014). TTP interacts with the decapping factor DCP2 (Fenger-Grøn et al., 2005), the CNOT1 subunit of the CCR4-NOT deadenylase complex (Fabian et al., 2013; Sandler et al., 2011), and the RNA-degrading exosome (Chen et al., 2001; Lykke-Andersen and Wagner, 2005). By recruiting these destabilizing activities, TTP mediates the rapid turnover of client mRNAs. TTP contains two RNA-binding zinc fingers that recognize adenylate-uridylate AU-rich elements (AREs) in the 3′ UTR of sensitive transcripts (Clark and Dean, 2016). When encountering inflammatory activators, this repressive mechanism is alleviated through the action of the p38/MK2 signaling axis and TTP phosphorylation, allowing for the rapid increase in mRNAs copies, which for some targets like that encoding TNF can be massive (Tiedje et al., 2014). This inactivation critically requires two MK2 phosphorylation sites on TTP, which mediates interaction with 14-3-3 proteins (Stoecklin et al., 2004; Tiedje et al., 2016). The binding of 14-3-3 may directly prevent the binding of TTP to mRNAs, the recruitment of destabilizing activities to the complex, or a combination of the two. As a direct consequence of its role as a suppressor of inflammatory signaling, loss of TTP in mice results in constitutively elevated levels of circulating cytokines and chronic inflammation (Taylor et al., 1996).

4EHP (EIF4E2) is an ortholog of the mRNA cap-binding and translation initiation factor EIF4E1, which is defective for binding to EIF4G and thus cannot assemble into a productive EIF4F initiation complex (Rom et al., 1998; Zuberek et al., 2007). As a result, 4EHP-bound mRNAs are translationally silenced, and this mechanism is required for perinatal viability in mice (Morita et al., 2012). 4EHP forms complexes with the GYF domain-containing proteins GIGYF1 and GIGYF2, which are critical for this translational repression (Peter et al., 2017). It has been proposed that GIGYFs act as scaffolds that link mRNA-binding proteins with 4EHP, providing target specificity in translational silencing. TTP is one such specificity factor, and at least part

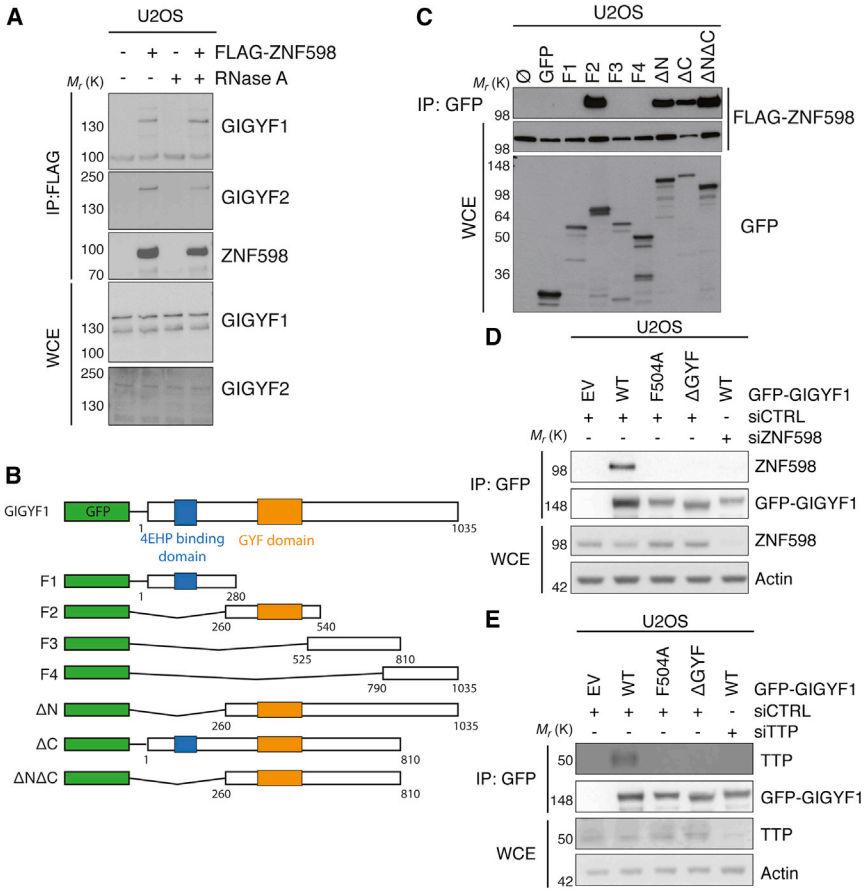

Figure 1. GIGYF1 Binds ZNF598 and TTP via GYF Domains

(A) U2OS cells were transfected with FLAG-ZNF598 plasmid. Lysates were treated with RNase A as indicated and subjected to FLAG immunoprecipitation, followed by immunoblotting with antibodies against GIGYF1, GIGYF2, and ZNF598.

(B) Schematic representation of GYGIF1 domain structure and GFP-tagged truncation constructs used in (C).

(C) U2OS cells were co-transfected with FLAG-ZNF598 construct and plasmids encoding GFP-GIGYF1 fragments from (B). Lysates were subjected to GFP immunoprecipitation followed by immunoblotting with antibodies against FLAG and GFP.

(D) U2OS cells were transfected with indicated siRNAs, and WT or mutant versions of GFP-GIGYF1 plasmid. Lysates were treated as in (C) and also blotted for actin.

(E) As in (D), except that cells were transfected with TTP siRNA and lysates were analyzed by immunoblotting with TTP antibody.

of the repression of pro-inflammatory gene expression occurs in the context of a 4EHP-GIGYF2-TTP complex (Fu et al., 2016; Tao and Gao, 2015). Apart from serving as mere scaffolding factors, GIGYF1/2 may also contribute directly to the translational repression of transcripts (Amaya Ramirez et al., 2018; Peter et al., 2017). GYF domains have high affinity for polyproline stretches, a feature shared with other protein-protein interaction domains such as the SH3 family (Kofler et al., 2009). TTP contains three proline clusters, and these are required for integrating TTP into the complex with 4EHP and GIGYF2 (Fu et al., 2016).

During the process of protein translation, the stalling of ribosomes triggers a conserved salvage pathway that disassembles these ribosomes and mediates ubiquitination, release, and degradation of the nascent peptide chain (Joazeiro, 2017). A large body of recent work identified the *Saccharomyces cerevisiae* ubiquitin ligase Hel2 and its mammalian counterpart ZNF598 as early responders in ribosome-associated quality control (RQC) (Garzia et al., 2017; Juszkiewicz and Hegde, 2017; Sundaramoorthy et al., 2017).

In previous work that uncovered translational repression by 4EHP and GIGYF proteins, ZNF598 was also found to be associated with these complexes (Morita et al., 2012). Similar to TTP, ZNF598 contains RNA-binding zinc fingers; we therefore investigated whether this protein could also have the potential for posttranscriptional gene regulation. Here, we show that ZNF598 binds GIGYF1/2 in a manner similar to that described for TTP and GIGYF2 (Fu et al., 2016) and that these two RNA-binding proteins share a number of mRNA-binding partners. ZNF598 deficiency is associated with the upregulation of a number of inflammation-associated transcripts, some of which are also regulated by TTP, including interleukin 8 (IL-8) and colony-stimulating factor 2 (CSF2) mRNA. Our results identify ZNF598 as a TTP-like factor in the posttranscriptional regulation of the inflammatory response, in addition to its established role in RQC.

RESULTS

GIGYF Proteins Bind ZNF598 and TTP via GYF Domains

Using co-immunoprecipitation in U2OS cells, we readily observed a strong interaction between ZNF598 and GIGYF1 when purifying FLAG-tagged ZNF598, GFP-tagged GIGYF1, and endogenous GIGYF1 (Figures 1A, S1A, and S1B). This observation could be extended to several human cell lines in which FLAG-ZNF598 co-purified with both GIGYF1 and GIGYF2, in accordance with previous work (Figures S1C and S1E) (Morita et al., 2012). These interactions were not mediated by RNA, as treatment of the lysates with an RNase A before immunoprecipitation did not ablate the binding (Figures 1A and S1C). By generating and analyzing a series of overlapping and N-terminally GFP-tagged fragments and deletion constructs of GIGYF1, we narrowed down the region responsible for ZNF598 binding to a fragment comprising the GYF domain (Figures 1B and 1C). We then proceeded to disable this domain in the context of full-length GIGYF1, either by deletion of the three signature amino acids (ΔGYF) or by single mutation of the phenylalanine (mutant F504A). These alterations completely abolished ZNF598 binding,

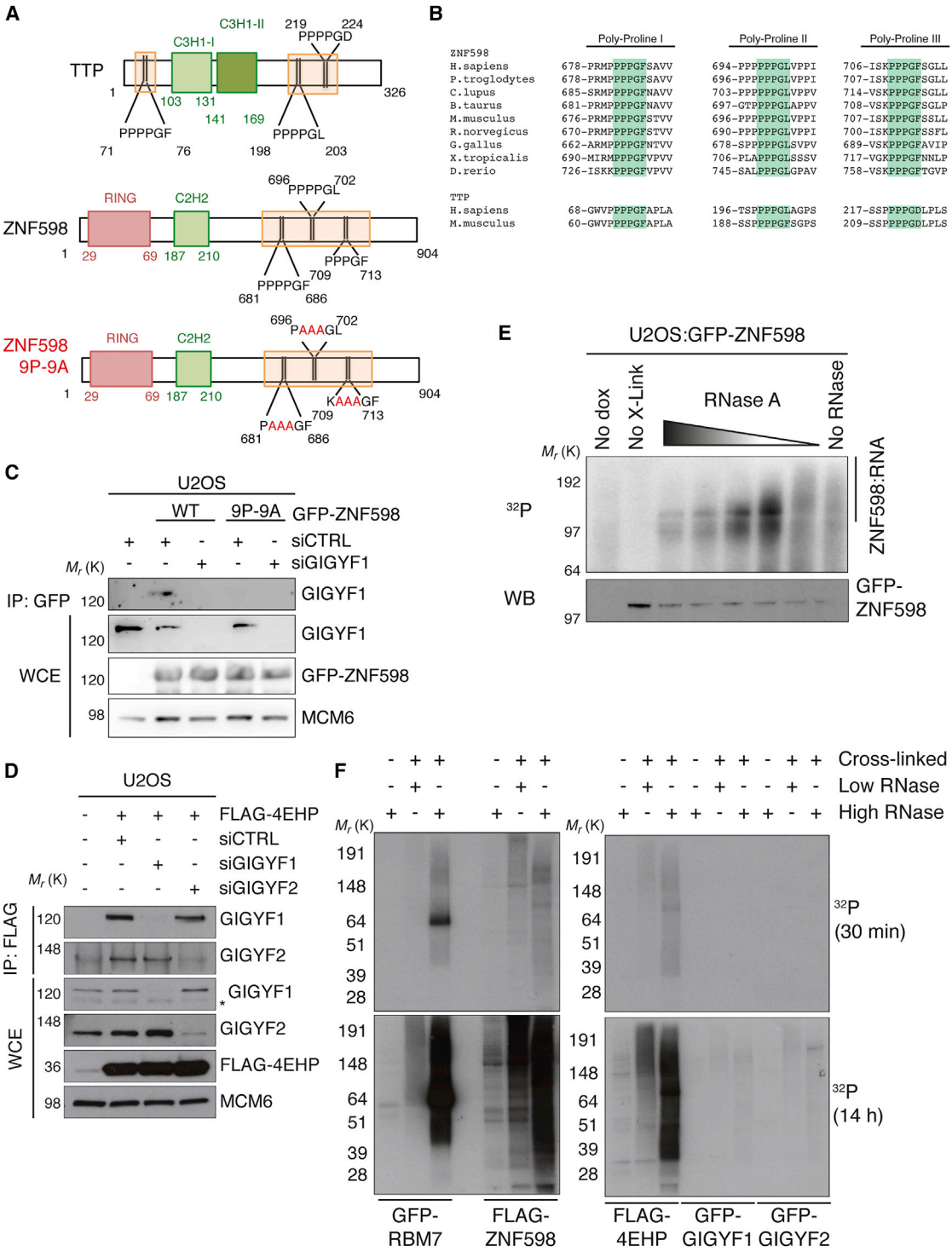

Figure 2. Architecture of 4EHP-GIGYF-RBP Complexes

(A) Domain structure of TTP and ZNF598. Notice the presence of zinc fingers (C3H1 and C2H2 types) and polyproline stretches in both proteins.

(B) Alignment of polyproline stretches from ZNF598 and TTP across species. H, Homo; P, Pan; C, Canis; B, Bos; M, Mus; R, Rattus; G, Gallus; X, *Xenopus*; and D, Danio.

(C) U2OS cells were transfected with indicated siRNAs and WT or proline-to-alanine substitution mutant versions of GFP-ZNF598 plasmid. Lysates were subjected to GFP immunoprecipitation, followed by immunoblotting with antibodies against GIGYF1, GFP, and minichromosome maintenance complex 6 (MCM6). WCE, whole-cell extract; IP, immunoprecipitation.

(legend continued on next page)

strongly suggesting that the GYF domain of GIGYF1 constitutes the ZNF598 binding domain (Figure 1D). It was recently suggested, although not formally proven, that the same domain is responsible for TTP interaction by contacting the signature proline stretches in this protein, and it was also shown that GYF and related domains have high affinity for such proline stretches (Fu et al., 2016; Kofler et al., 2009). We were able to corroborate these findings by showing that the above-mentioned GYF domain mutants of GIGYF1 were completely defective for TTP binding (Figures 1E and S1D).

Given the overlapping requirements of the GIGYF1 GYF domain for binding to both ZNF598 and TTP, we analyzed the amino acid sequence of ZNF598 for the presence of polyproline stretches. We spotted three such clusters in the C-terminal half of ZNF598, which were conserved all the way to zebrafish, and even in the surrounding amino acids they bear a strong resemblance to the polyproline stretches in TTP (Figures 2A and 2B). When the last three prolines in each of these clusters were mutated to alanines, the binding of ZNF598 to GIGYF1 and GIGYF2 was completely abolished (Figures 2C and S1E). The same strict requirement for the polyproline stretches in TTP for interaction with GIGYF proteins was shown recently (Fu et al., 2016), and together with our own observations, suggests that ZNF598 and TTP have remarkable structural similarities and display equivalent modes of interaction with GIGYF proteins.

Hierarchical Complex Formation between 4EHP, GIGYF1, and RNA-Binding Factors TTP and ZNF598

To further characterize the architecture of GIGYF-containing complexes, we performed a series of pull-down experiments. When purifying FLAG-tagged 4EHP, we readily detected interactions with endogenous GIGYF1 and GIGYF2, in full agreement with the published literature (Morita et al., 2012; Peter et al., 2017). These interactions appeared to be independent, as GIGYF2 was not required for the interaction of GIGYF1 with 4EHP and vice versa (Figure 2D). In fact, while both GFP-GIGYF1 and GFP-GIGYF2 readily co-purified FLAG-4EHP, we could not detect any co-purification of GIGYF2 and GIGYF1, suggesting that these two proteins form independent complexes with 4EHP (Figures S1F and S1G).

The primary sequence of ZNF598 reveals the presence of potential RNA-binding domains. In fact, in addition to the annotated C2H2-type zinc finger in its N-terminal half (Figure 2A), putative zinc finger domains can be spotted throughout the sequence of ZNF598 (Garzia et al., 2017). We thus surmised that, similar to TTP, ZNF598 could be an RNA-binding protein, and we addressed this by cross-linking immunoprecipitation (CLIP) experiments (König et al., 2012). In support of our hypothesis, GFP-ZNF598 co-purified RNA from UV-cross-linked cells, resulting in a smear of radioactivity-labeled bands running above the expected molecular weight of GFP-ZNF598. Treatment of the cross-linked extracts with increasing amounts of RNase gradually collapsed these bands to the expected molecular weight of GFP-ZNF598, suggesting that ZNF598 directly binds RNA species in cells (Figure 2E). Together with the previous results, these findings suggest the existence of hierarchical and mutually exclusive complexes between the cap-binding protein 4EHP, scaffolding factors GIGYF1 and GIGYF2, and RNA-binding proteins (RBPs) such as TTP, ZNF598, and potentially others, each with the potential to regulate translation and/or turnover of specific transcripts. We also used the CLIP approach combined with the purification of GIGYF1 and GIGYF2, but in neither case did we observe a radioactive signal to indicate direct RNA interaction of these factors. Conversely, 4EHP and the control RNA-binding motif 7 (RBM7) (Lubas et al., 2015) strongly cross-linked to RNA under these experimental settings, suggesting to us that RNA-binding activity within these complexes is restricted to 4EHP, TTP, and ZNF598 (Figure 2F).

ZNF598 Suppresses Inflammation-Associated mRNAs

To elucidate a potential role for ZNF598 in posttranscriptional gene regulation, we proceeded to perform RNA sequencing (RNA-seq) from cell extracts. We used standard methods to produce four cDNA sequencing libraries in independent biological duplicates from cells transfected with either a mismatch control or ZNF598-targeting small interfering RNA (siRNA) and incubated or not with IL-1β for 1 h (Figures 3A and S2A). Sequencing of the eight libraries each resulted in approximately 50 million reads that could be mapped to the genome and formed the basis for differential expression analysis. This revealed the existence of a substantial number of transcripts, the abundances of which were sensitive to ZNF598 depletion under resting and IL-1β stimulation conditions (Figure 3B; Table S1). By determining the overlap of ZNF598-regulated genes under these two conditions, it became clear that >50% of all deregulated genes are decoupled from IL-1β stimulation (Figure 3B). Furthermore, we realized that many genes exclusively deregulated under resting conditions (317) are associated with inflammation (Figure S2B), pointing toward a mode of action similar to TTP. Almost 40% of all targets induced by IL-1β stimulation in control cells are part of this subset of transcripts (Figure 3C). We proceeded to conduct a

(D) U2OS cells were transfected with indicated siRNAs and FLAG-4EHP plasmid. Lysates were subjected to FLAG immunoprecipitation, followed by immunoblotting with antibodies against GIGYF1, GIGYF2, FLAG, and MCM6. Asterisk denotes unspecific band.

(E) U2OS cells inducibly expressing GFP-ZNF598 were induced with doxycycline (dox) for 12 h, treated with UV-C (175 J/m^2), and immediately lysed. GFP-ZNF598 was immobilized on GFP beads, treated with increasing amounts of RNase A, and subjected to phosphorylation by polynucleotide 5′-hydroxyl kinase (PNK) in the presence of radioactive ATP. The material was released from the beads by boiling, separated by SDS-PAGE, and blotted onto a nitrocellulose membrane. Radioactive signals were measured by autoradiography. Input samples were transferred onto a nitrocellulose membrane and immunoblotted with GFP antibodies.

(F) U2OS cells were transfected with the indicated plasmids, cross-linked with a high dose of UV-C (175 J/m^2) and immediately lysed. GFP- and FLAG-tagged proteins were immobilized on beads, treated with either a high or a low concentration of RNase, and subjected to phosphorylation by T4-PNK in the presence of radioactive ATP. The material was released from the beads by boiling, separated by SDS-PAGE, and blotted onto a nitrocellulose membrane. Radioactive signals were measured by autoradiography. GFP-RBM7 was used as positive control.

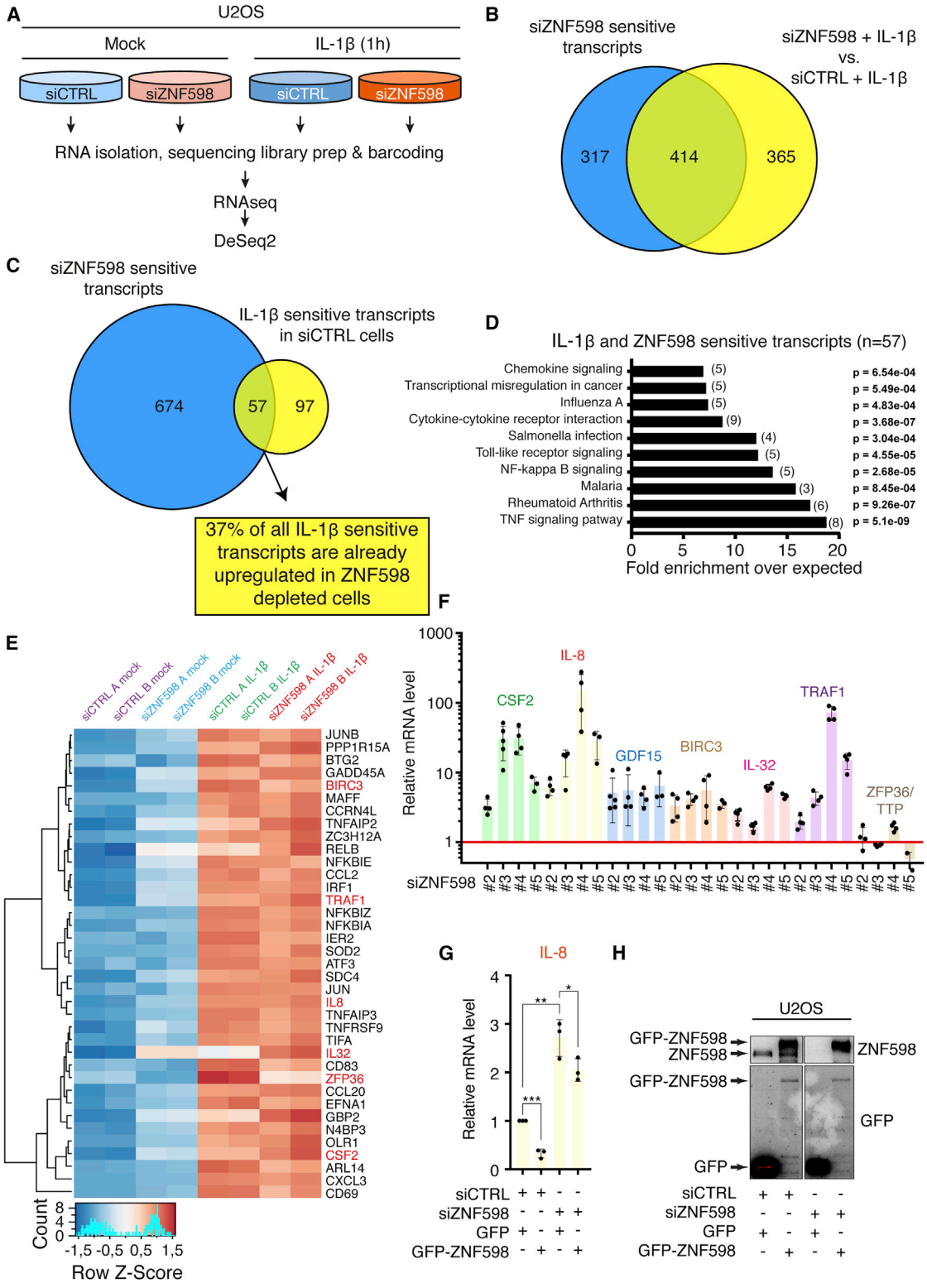

Figure 3. RNA-Seq Reveals Regulation of Inflammatory Transcripts by ZNF598

(A) Experimental setup for total RNA-seq. U2OS cells were transfected with the indicated siRNAs and stimulated with IL-1β for 1 h, as indicated (2 biological replicates). Cells were lysed, and the RNA was isolated and converted to barcoded cDNA libraries that were subjected to sequencing.

(legend continued on next page)

pathway overrepresentation analysis for these overlapping transcripts (Figure 3D) and for the ZNF598-sensitive transcripts under resting conditions (Figure S2B) using the WebGestalt (Zhang et al., 2005) interface. This revealed that in the absence of ZNF598, deregulated transcripts were associated with inflammation and immune signaling (Figures 3D and S2B). Since IL-1β stimulation is known to massively upregulate inflammation-associated RNAs (Dinarello, 2011), we next asked how strong the deregulation by ZNF598-depletion under resting conditions is, compared to after IL-1β stimulation. As seen in a clustered heatmap, the depletion of ZNF598 upregulated the depicted transcripts only moderately but consistently for this selected group (Figure 3E). It can also be seen that the differences are uncoupled upon IL-1β stimulation, suggesting that ZNF598 regulates inflammation-associated transcripts under resting conditions. To further validate these findings, we depleted ZNF598 with three additional and independent siRNAs (Figure S2C) and performed qPCR analysis for upregulated transcripts from our RNA-seq experiment. Transfection of each of these siRNAs was broadly accompanied by an increase in the levels of inflammation-associated mRNAs (Figure 3F). Of note, we did not observe any deregulation of TTP/ZFP36, which is considered the master regulator of (pro)-inflammatory mRNAs (Figure 3F). We could partially rescue these effects by transient transfection of exogenous and siRNA-resistant ZNF598 into ZNF598-depleted cells (Figures 3G, 3H, and S2D), allowing us to conclude that this RBP negatively regulates the abundance of a subset of transcripts.

Several of the ZNF598-regulated transcripts, including IL-8 and CSF2 mRNA (Figures 4A and 4B), are also established TTP targets, and we surmised that our analysis indicated that ZNF598, like TTP, is required for the suppression of pro-inflammatory signaling in resting cells. This was further underscored by the fact that the majority of mRNAs that increased upon IL-1β stimulation were already elevated after ZNF598 knockdown in our RNA-seq experiment (Figures 3E, 4A, and 4B), and we thus attempted to reproduce these effects by qPCR analysis. In these experiments, the basal levels of IL-8 and CSF2 transcripts were elevated in ZNF598 siRNA-treated cells, but displayed a normal level of induction following IL-1β stimulation (Figures 4C and 4D). We also constructed a cell line that allows for doxycycline-induced expression of mitogen-activated protein kinase kinase 6 (MKK6) and ensuing activation of p38 and MK2 (Figures S2E and S2F) to study the regulation of inflammatory transcripts. Under these experimental conditions, IL-8 mRNA was substantially increased after MKK6 induction in an MK2-dependent manner. While not required for this reaction, siRNA-mediated depletion of ZNF598 was accompanied by increased basal levels of IL-8 transcript (Figure S2F). Finally, we compared the sensitivity of the above transcripts to TTP and ZNF598 depletion, respectively. These interventions led to a comparable elevation of IL-8 and CSF2 mRNA levels, confirming that they are targets for TTP-mediated degradation and that, at least in U2OS cells, they are controlled to a similar degree by both RBPs (Figures 4E and 4F). ZNF598 may regulate mRNA abundance in a manner similar to TTP, and at least for IL-8 and CSF2 mRNA, ZNF598 knockdown decreased the turnover rate upon actinomycin D-induced transcriptional blockade (Figure S2G). Our RNA-seq experiments also revealed known TTP targets such as tumor necrosis factor (TNF) mRNA that were not sensitive to ZNF598 depletion, yet still enhanced upon IL-1β stimulation (Figure S3A). These experiments highlight the existence of a ZNF598-regulated transcript pool that is associated with inflammatory signaling and partly overlapping with the TTP-sensitive transcriptome.

ZNF598 Binds to IL-8 mRNA

Our data suggest that ZNF598, similar to TTP, is involved in the regulation of inflammatory transcripts in the context of 4EHP-GIGYF1/2-ZNF598 complexes. To corroborate our findings, we used RNA immunoprecipitation (RIP) to detect associations between ZNF598 and specific transcripts. We purified GFP-ZNF598 and GFP-TTP from cell lysates and probed the associated RNA content by qPCR for the presence of IL-8 transcript, the abundance of which we found to be regulated by both ZNF598 and TTP (Figure 4E). Even though this transcript is present in very small amounts in unstimulated cells (Winzen et al., 1999), we were able to reliably amplify it from both the GFP-ZNF598 and GFP-TTP associated RNA pool (Figure 5A), producing amplicons of the expected molecular weight (Figure 5B). Conversely, TNF mRNA, the levels of which were not regulated by ZNF598 but were increased upon IL-1β stimulation (Figure S3A), could only be amplified from TTP pull-downs (Figures 5A and 5B), underscoring the partial nature of the overlap between TTP and ZNF598 client mRNAs. To further characterize the RNA-binding properties of ZNF598, we used an RNA-electrophoretic mobility shift assay (REMSA) strategy. We purified strep-ZNF598 and strep-TTP from HEK293T cells (Figures S4A–S4C) and evaluated the ability of these proteins to induce a mobility shift of a 60-base fragment of the 3′ UTR of IL-8

(B) Venn diagram illustrating the overlap between ZNF598-sensitive transcripts in non-stimulated cells (siZNF598 versus siCTRL, 731 transcripts) and transcripts upregulated upon IL-1β treatment in both siCTRL and siZNF598 cells (siZNF598 + IL-1β versus siCTRL + IL-1β, 779 transcripts).
(C) Venn diagram showing the overlap between IL-1β-sensitive transcripts in resting cells (siCTRL + IL-1β versus siCTRL, 154 transcripts) and ZNF598-sensitive transcripts (siZNF598 versus siCTRL, 731 transcripts).
(D) Pathway overrepresentation analysis of 57 IL-1β-induced transcripts that are constitutively upregulated in ZNF598-depleted cells (overlapping area in C), deduced with the WebGestalt tool (Zhang et al., 2005). Numbers in brackets indicate the number of genes enriched clustering to the corresponding pathway.
(E) Clustered heatmap of ZNF598-sensitive transcripts involved in the IL-1β-induced inflammatory response. Transcripts highlighted in red were used for subsequent validation experiments.
(F) U2OS cells were transfected with four independent ZNF598 siRNAs (#2–#5). Upon cell lysis, total RNA was recovered, and the relative abundance of indicated mRNAs was determined by qPCR. Black dots indicate individual measurements; bars indicate the means ± SDs from 3–5 technical replicates.
(G) U2OS cells were transfected with indicated siRNAs and siRNA-resistant GFP-ZNF598. Upon cell lysis, total RNA was recovered, and the relative abundance of IL-8 mRNA was determined by qPCR. Black dots indicate measurements of three biological replicates. Bars indicate means ± SDs.
(H) Lysates from (G) were analyzed by immunoblotting with antibodies against ZNF598 and GFP.

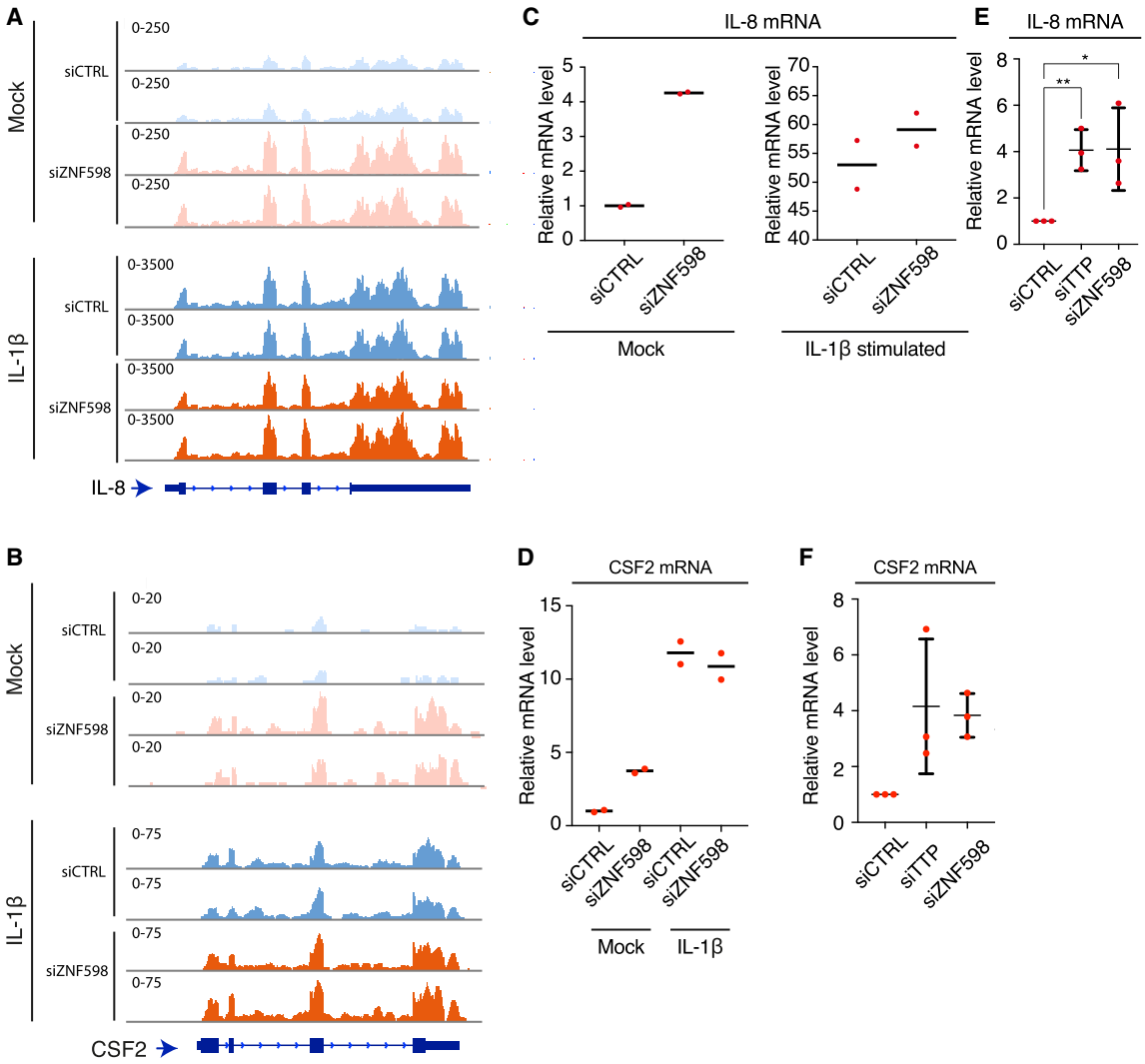

Figure 4. ZNF598 and TTP Control the Abundance of IL-8 and CSF2 Transcripts

(A) Mapping of sequencing reads to the IL-8 gene from two biological replicates of the experiment outlined in Figure 3A. Note the difference in scale used for mock versus IL-1β-treated samples. IL-8 transcript structure is indicated below the profiles. The arrow denotes the location of the start codon, and the increasing thickness of the line represents introns, untranslated regions, and exons, respectively.

(B) As in (A), except that reads were mapped to the CSF2 gene.

(C) U2OS cells were transfected with siRNAs and treated with IL-1β (1 h), as indicated. Upon cell lysis, total RNA was recovered, and the relative abundance of IL-8 mRNA was determined by qPCR. Red dots indicate measurements from two biological replicates. Bars indicate the means.

(D) As in (C), except that CSF2 mRNA abundance was measured.

(E) U2OS cells were transfected with indicated siRNAs. Upon cell lysis, total RNA was recovered, and the relative abundance of IL-8 mRNA was determined by qPCR. Red dots indicate the measurements from three biological replicates.

(F) As in (E), except that CSF2 mRNA abundance was measured.

mRNA, which was previously annotated as the minimal TTP-binding region (Figure 5C) (Winzen et al., 2007). In both cases, pre-incubation with increasing amounts of protein resulted in the gradual depletion of free RNA probe and recovery of the fluorescence signal in a mobility-retarded form, which is indicative of an RNA-protein complex. Quantification of the band intensities indicated a similar affinity of the two RBPs toward the RNA probe (Figure 5D). These results indicate that ZNF598, like TTP, can bind the 3′ UTR of IL-8, even in an *in vitro* setting. The interaction is likely to be direct, as the mutant of ZNF598 that cannot associate with the 4EHP-GIGYF module (9P-9A) bound the probe with similar affinity (Figures 5E, S4D, and S4E); however, we cannot formally exclude the possibility that these interactions are mediated by factors co-purifying with wild-type (WT) and mutant GFP-ZNF598. We also used this assay to evaluate the contribution of the different RNA-binding regions in ZNF598 to IL-8 mRNA binding. Our deletion analysis indicated that both N- and C-terminal sequences in ZNF598 are involved in RNA

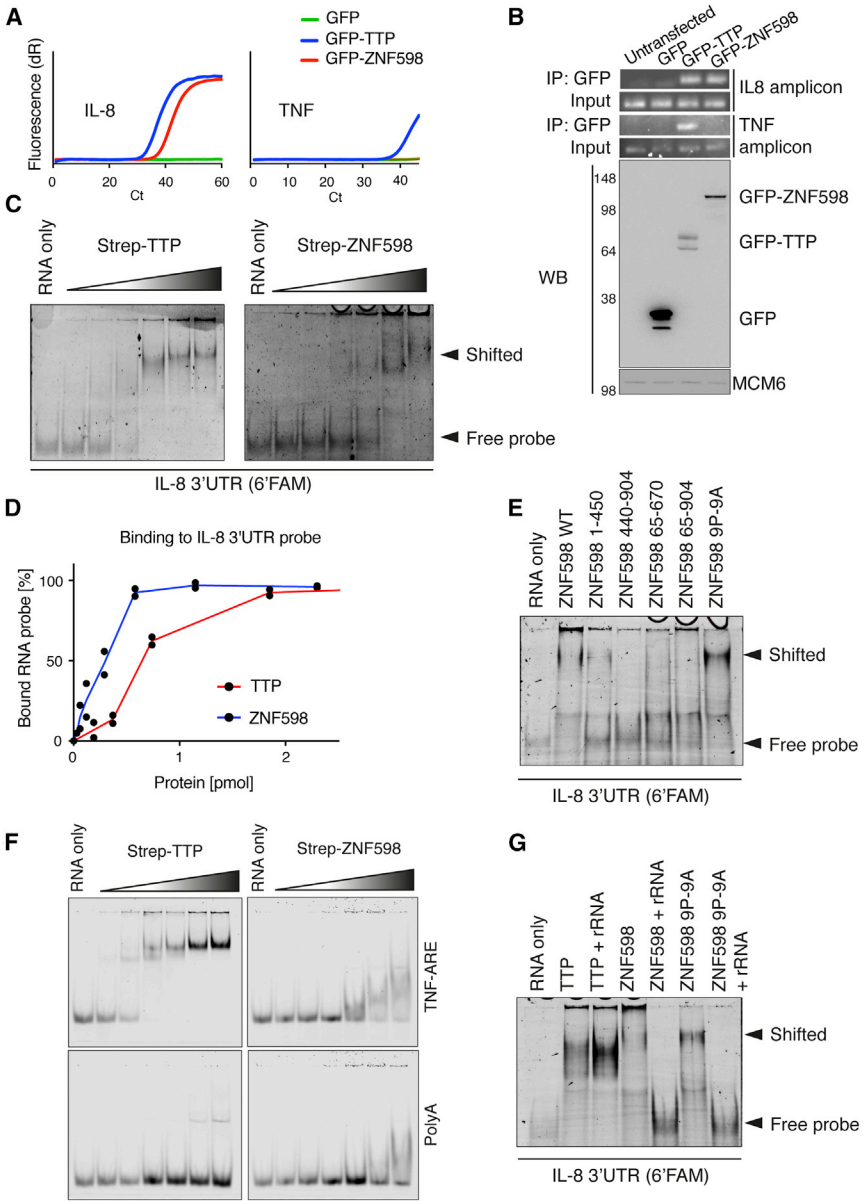

Figure 5. ZNF598 Binds Directly to IL-8 Transcript

(A) U2OS cells were transfected with indicated GFP plasmids, lysed, and subjected to GFP immunoprecipitation. RNA species were reclaimed from the beads, converted to cDNA, and analyzed by qPCR, with primers against IL-8 and TNF. Ct, cycle threshold.

(B) Input RNA and qPCR-amplified material from (A) were separated on agarose gels and stained for DNA content, producing PCR fragments of the expected sizes. Input lysates were analyzed by immunoblotting, with antibodies against GFP and MCM6. WB, western blot.

(C) A fluorescently tagged RNA fragment comprising 60 bases from the IL-8 3′ UTR was incubated with increasing amounts of purified strep-TTP (left) or strep-ZNF598 (right). Reaction mixtures were separated by gel electrophoresis under non-denaturing conditions and fluorescent signals recorded. 6'FAM, 6-carboxyfluorescein.

(D) Estimation of ZNF598 and TTP affinity toward the IL-8 3′ UTR probe was calculated based on fluorescence signal of the bands in (C), and the protein concentrations were estimated from Figure S4C. Data points represent the mean of two biological replicates for ZNF598 and TTP.

(E) As in (C), except that the IL-8 probe was incubated with deletion constructs and mutants of strep-tagged ZNF598.

(F) As in (C), except that purified strep-TTP and strep-ZNF598 were incubated with RNA probes from the 3′ UTR of TNF (top) or a polyA probe (bottom).

(G) Strep-TTP and strep-ZNF598 were incubated with the IL-8 probe and an excess of bacterial ribosomal RNA, as indicated. Reaction mixtures were analyzed as in (C).

binding (Figures 5E, S4D, and S4E), which is in agreement with previous publications (Garzia et al., 2017). To test whether the RNA interaction of ZNF598 is target specific, we performed the same experiments with the 3′ UTR ARE from TNF as a probe. Only TTP incubation resulted in a mobility shift of this probe (Figure 5F, top), which is consistent with our RIP experiments (Figures 5A and 5B). Furthermore, and serving as an important control, neither ZNF598 nor TTP bound strongly to a polyA probe (Figure 5F, bottom). The lack of a clear and unique determinant for RNA binding in ZNF598 (Figure 5E) prompted us to further characterize the RNA-binding properties of ZNF598 and TTP. While TTP displays a strong preference for 3′ AREs both *in vivo* and *in vitro*, photo-activatable ribonucleoside (PAR)-CLIP analysis suggested that ZNF598 has no such preference and binds to several species of RNA and in coding and noncoding regions of mRNAs (Garzia et al., 2017). This lack of sequence stringency was underscored by the fact that we could compete out the binding of ZNF598 to the IL-8 probe with high amounts of bacterial ribosomal RNA, while under the same conditions, TTP remained bound to its target RNA (Figure 5G). These results indicate that, although they may share a number of mRNA targets, ZNF598 and TTP differ greatly in their modes of RNA interaction.

Overlap between ZNF598-Regulated and -Interacting RNAs

Taking advantage of a recently published ZNF598 PAR-CLIP dataset (Garzia et al., 2017), we also assessed to what degree ZNF598 interacting transcripts were sensitive to ZNF598 depletion in our RNA-seq experiments (Figure S5A). To this end, we compared our set of strongest (log2-fold >1 and <1) and significant (p-adj $\leq$ 0.05) ZNF598-sensitive transcripts in U2OS cells to the mRNAs significantly enriched in the PAR-CLIP dataset (with the potential caveat that these data were generated from HEK293T cells). This analysis indicated that roughly 10% of

the ZNF598-sensitive transcripts are also PAR-CLIP targets of ZNF598 (Figure S5A; Table S2). Of note, when we compared the same set of ZNF598-sensitive targets to a list of TTP interactors identified by PAR-CLIP in HEK293T (Mukherjee et al., 2014), the overlap was only 2% (data not shown). Furthermore, when narrowing our analysis to transcripts that were detected both in our RNA-seq experiments in U2OS cells and the previously published ZNF598 PAR-CLIP dataset from HEK cells, we observed that 66.6% of the transcripts showing a high CLIP occupancy (>95th percentile) were sensitive to ZNF598 depletion (Figures S5B and S5C; Table S3).

Our results suggest that ZNF598, like TTP, functions as an RBP in a complex with 4EHP and GIGYFs, which confers posttranscriptional control over a subset of inflammation-associated transcripts.

DISCUSSION

In this study, we have uncovered a role for ZNF598 in posttranscriptional gene regulation. ZNF598 is an RBP with the capacity to directly interact with rRNA as well as mRNA species, a subset of which encode mediators of inflammatory signaling. The depletion of ZNF598 was associated with the upregulation of a broad range of inflammation-associated mRNAs, including the IL-8 transcript, for which we could also demonstrate direct binding to ZNF598. We also highlighted how ZNF598 and TTP share a number of structural features such as polyproline stretches that bind the GYF domain of GIGYF proteins and integrate these RBPs into larger 4EHP-GIGYF1/2-RBP translation initiation inhibitory complexes. There is an overlap between the mRNAs that are targeted by ZNF598 and TTP (e.g., IL-8, CSF2 mRNA). TNF mRNA, however, appears to be a unique TTP target that is neither bound nor regulated by ZNF598. Besides functionally separating ZNF598 and TTP, the lack of TNF mRNA stabilization upon ZNF598 depletion also signifies that the induction of other inflammatory markers is not merely a TTP-dependent response to our experimental interventions. While TTP predominantly binds ARE sequences in the 3′ UTR, ZNF598 binding sequences appear both to be more cryptic in nature and can be located in coding and noncoding regions of mRNAs. ZNF598 binding to target RNAs correlates with their regulation at the mRNA level to a certain extent.

In the case of TTP, the mechanisms governing target repression have been the subject of a number of studies (Clark and Dean, 2016). On the one hand, TTP mediates the rapid turnover of client mRNAs in resting cells, and this mechanism is abrogated upon inflammatory stimuli in a manner dependent on MK2-mediated phosphorylation and ensuing 14-3-3 binding of TTP (Clark and Dean, 2016; Stoecklin et al., 2004; Tiedje et al., 2016). On the other hand, TTP confers negative translational control over mRNAs in the context of the 4EHP-GIGYF complex (Fu et al., 2016; Peter et al., 2017; Tao and Gao, 2015). How ZNF598 regulates target mRNAs acting within and outside the inflammatory response remains to be investigated in detail, but also in this case, the mechanism is likely to involve the destabilization of client mRNAs and translational repression. We could show that the half-life of IL-8 and CSF2 transcripts is enhanced in the absence of ZNF598.

The ubiquitin ligase function of mammalian ZNF598 was recently shown to be critically required for ribosome ubiquitination and RQC (Garzia et al., 2017; Juszkiewicz and Hegde, 2017; Sundaramoorthy et al., 2017). This function is conserved from its distant *S. cerevisiae* homolog Hel2. Of note, TTP and GIGYF1/2 do not have budding yeast homologs, and when we inspected the primary structure of Hel2, we did not observe a conservation of the polyproline stretches that in mammalian ZNF598 bind GIGYF1/2. This suggests to us that the posttranscriptional gene regulatory function of ZNF598, or at least its integration into translation inhibitory complexes, is a more recent evolutionary invention that likely coincided with the appearance of the GIGYF proteins. In this context, it is interesting that only a small part of the cellular pool of ZNF598 associates with translating ribosomes, and that deletion mutants defective for ribosome binding still retain the ability to bind RNA (Garzia et al., 2017). Such results support our proposal of an additional role for ZNF598, in addition to its established function during RQC.

Our data establish ZNF598 as a posttranscriptional regulator of gene expression and suppressor of inflammatory signaling. Whether this role of ZNF598 has implications for the function of the immune system and/or human health remains to be established. Efforts toward this end will be hampered by the likely profound defects associated with a compromised RQC, and the establishment of separation-of-function mutants of ZNF598 will be crucial to initiate such studies. In conclusion, our findings significantly add to the present knowledge of regulatory mechanisms that control inflammatory signaling in cells.

STAR★METHODS

Detailed methods are provided in the online version of this paper and include the following:

- KEY RESOURCES TABLE
- CONTACT FOR REAGENT AND RESOURCE SHARING
- EXPERIMENTAL MODEL AND SUBJECT DETAILS
- METHOD DETAILS
  - Plasmids and siRNAs
  - Cell culture and reagents
  - Immunochemical methods
  - CLIP
  - Quantitative (q)PCR
  - RNA-sequencing, mapping and differential gene expression analysis
  - PAR-CLIP
  - RNA electrophoretic mobility shift assay (REMSA)
- QUANTIFICATION AND STATISTICAL ANALYSIS
- DATA AND SOFTWARE AVAILABILITY

SUPPLEMENTAL INFORMATION

Supplemental Information can be found online at https://doi.org/10.1016/j.celrep.2019.03.006.

ACKNOWLEDGMENTS

We thank Dr. Nahum Sonenberg (McGill University, Canada) for providing reagents and Drs. Helen Michéle Neil and Andreas Mund (University of

Copenhagen, Denmark) for help with RNA-seq. Work in the Bekker-Jensen lab was supported by grants from the Lundbeck Foundation, the NEYE Foundation, and The Danish Medical Research Council. T.S.B. is funded by the HOPE project grant from the Novo Nordisk Foundation (grant number NNF17SA0027704). Work at the Novo Nordisk Foundation Center for Protein Research (CPR) is funded in part by a generous donation from the Novo Nordisk Foundation (grant number NNF14CC0001).

AUTHOR CONTRIBUTIONS

M.A.X.T., C.T., J.C.N., A.C.V., and M.B. performed the biochemical and cell biological experiments. T.S.B. and J.V.O. performed and analyzed the proteomics experiments. S.R. and C.T. generated and analyzed the sequencing data and performed the bioinformatics analyses. N.M. and M.G. helped conceive the project and analyze the data. M.A.X.T. and S.B.-J. designed the experiments, conceived the project, and wrote the manuscript. All of the authors discussed the results and commented on the manuscript.

DECLARATION OF INTERESTS

The authors declare no competing interests.

Received: December 15, 2017
Revised: January 3, 2019
Accepted: February 27, 2019
Published: March 26, 2019

REFERENCES

Afgan, E., Baker, D., Batut, B., van den Beek, M., Bouvier, D., Cech, M., Chilton, J., Clements, D., Coraor, N., Grüning, B.A., et al. (2018). The Galaxy platform for accessible, reproducible and collaborative biomedical analyses: 2018 update. Nucleic Acids Res. *46* (*W1*), W537–W544.

Althammer, S., González-Vallinas, J., Ballaré, C., Beato, M., and Eyras, E. (2011). Pyicos: a versatile toolkit for the analysis of high-throughput sequencing data. Bioinformatics *27*, 3333–3340.

Amaya Ramirez, C.C., Hubbe, P., Mandel, N., and Béthune, J. (2018). 4EHP-independent repression of endogenous mRNAs by the RNA-binding protein GIGYF2. Nucleic Acids Res. *46*, 5792–5808.

Chen, C.Y., Gherzi, R., Ong, S.E., Chan, E.L., Raijmakers, R., Pruijn, G.J., Stoecklin, G., Moroni, C., Mann, M., and Karin, M. (2001). AU binding proteins recruit the exosome to degrade ARE-containing mRNAs. Cell *107*, 451–464.

Clark, A.R., and Dean, J.L. (2016). The control of inflammation via the phosphorylation and dephosphorylation of tristetraprolin: a tale of two phosphatases. Biochem. Soc. Trans. *44*, 1321–1337.

Cunningham, F., Amode, M.R., Barrell, D., Beal, K., Billis, K., Brent, S., Carvalho-Silva, D., Clapham, P., Coates, G., Fitzgerald, S., et al. (2015). Ensembl 2015. Nucleic Acids Res. *43*, D662–D669.

Dinarello, C.A. (2011). Interleukin-1 in the pathogenesis and treatment of inflammatory diseases. Blood *117*, 3720–3732.

Fabian, M.R., Frank, F., Rouya, C., Siddiqui, N., Lai, W.S., Karetnikov, A., Blackshear, P.J., Nagar, B., and Sonenberg, N. (2013). Structural basis for the recruitment of the human CCR4-NOT deadenylase complex by tristetraprolin. Nat. Struct. Mol. Biol. *20*, 735–739.

Fenger-Grøn, M., Fillman, C., Norrild, B., and Lykke-Andersen, J. (2005). Multiple processing body factors and the ARE binding protein TTP activate mRNA decapping. Mol. Cell *20*, 905–915.

Fu, R., Olsen, M.T., Webb, K., Bennett, E.J., and Lykke-Andersen, J. (2016). Recruitment of the 4EHP-GYF2 cap-binding complex to tetraproline motifs of tristetraprolin promotes repression and degradation of mRNAs with AU-rich elements. RNA *22*, 373–382.

Garzia, A., Jafarnejad, S.M., Meyer, C., Chapat, C., Gogakos, T., Morozov, P., Amiri, M., Shapiro, M., Molina, H., Tuschl, T., and Sonenberg, N. (2017). The E3 ubiquitin ligase and RNA-binding protein ZNF598 orchestrates ribosome quality control of premature polyadenylated mRNAs. Nat. Commun. *8*, 16056.

Gerstberger, S., Hafner, M., and Tuschl, T. (2014). A census of human RNA-binding proteins. Nat. Rev. Genet. *15*, 829–845.

Hansen, H.T., Rasmussen, S.H., Adolph, S.K., Plass, M., Krogh, A., Sanford, J., Nielsen, F.C., and Christiansen, J. (2015). Drosophila Imp iCLIP identifies an RNA assemblage coordinating F-actin formation. Genome Biol. *16*, 123.

Joazeiro, C.A.P. (2017). Ribosomal Stalling During Translation: Providing Substrates for Ribosome-Associated Protein Quality Control. Annu. Rev. Cell Dev. Biol. *33*, 343–368.

Juszkiewicz, S., and Hegde, R.S. (2017). Initiation of Quality Control during Poly(A) Translation Requires Site-Specific Ribosome Ubiquitination. Mol. Cell *65*, 743–750.e4.

Kofler, M., Schuemann, M., Merz, C., Kosslick, D., Schlundt, A., Tannert, A., Schaefer, M., Lührmann, R., Krause, E., and Freund, C. (2009). Proline-rich sequence recognition: I. Marking GYF and WW domain assembly sites in early spliceosomal complexes. Mol. Cell. Proteomics *8*, 2461–2473.

König, J., Zarnack, K., Luscombe, N.M., and Ule, J. (2012). Protein-RNA interactions: new genomic technologies and perspectives. Nat. Rev. Genet. *13*, 77–83.

Love, M.I., Huber, W., and Anders, S. (2014). Moderated estimation of fold change and dispersion for RNA-seq data with DESeq2. Genome Biol. *15*, 550.

Lubas, M., Andersen, P.R., Schein, A., Dziembowski, A., Kudla, G., and Jensen, T.H. (2015). The human nuclear exosome targeting complex is loaded onto newly synthesized RNA to direct early ribonucleolysis. Cell Rep. *10*, 178–192.

Lykke-Andersen, J., and Wagner, E. (2005). Recruitment and activation of mRNA decay enzymes by two ARE-mediated decay activation domains in the proteins TTP and BRF-1. Genes Dev. *19*, 351–361.

Morita, M., Ler, L.W., Fabian, M.R., Siddiqui, N., Mullin, M., Henderson, V.C., Alain, T., Fonseca, B.D., Karashchuk, G., Bennett, C.F., et al. (2012). A novel 4EHP-GIGYF2 translational repressor complex is essential for mammalian development. Mol. Cell. Biol. *32*, 3585–3593.

Mukherjee, N., Jacobs, N.C., Hafner, M., Kennington, E.A., Nusbaum, J.D., Tuschl, T., Blackshear, P.J., and Ohler, U. (2014). Global target mRNA specification and regulation by the RNA-binding protein ZFP36. Genome Biol. *15*, R12.

Okumura, F., Zou, W., and Zhang, D.E. (2007). ISG15 modification of the eIF4E cognate 4EHP enhances cap structure-binding activity of 4EHP. Genes Dev. *21*, 255–260.

Peter, D., Weber, R., Sandmeir, F., Wohlbold, L., Helms, S., Bawankar, P., Valkov, E., Igreja, C., and Izaurralde, E. (2017). GIGYF1/2 proteins use auxiliary sequences to selectively bind to 4EHP and repress target mRNA expression. Genes Dev. *31*, 1147–1161.

Plass, M., Rasmussen, S.H., and Krogh, A. (2017). Highly accessible AU-rich regions in 3′ untranslated regions are hotspots for binding of regulatory factors. PLoS Comput. Biol. *13*, e1005460.

Richardson, J.E. (2006). fjoin: simple and efficient computation of feature overlaps. J. Comput. Biol. *13*, 1457–1464.

Rom, E., Kim, H.C., Gingras, A.C., Marcotrigiano, J., Favre, D., Olsen, H., Burley, S.K., and Sonenberg, N. (1998). Cloning and characterization of 4EHP, a novel mammalian eIF4E-related cap-binding protein. J. Biol. Chem. *273*, 13104–13109.

Sandler, H., Kreth, J., Timmers, H.T., and Stoecklin, G. (2011). Not1 mediates recruitment of the deadenylase Caf1 to mRNAs targeted for degradation by tristetraprolin. Nucleic Acids Res. *39*, 4373–4386.

Stoecklin, G., Stubbs, T., Kedersha, N., Wax, S., Rigby, W.F.C., Blackwell, T.K., and Anderson, P. (2004). MK2-induced tristetraprolin:14-3-3 complexes prevent stress granule association and ARE-mRNA decay. EMBO J. *23*, 1313–1324.

Sundaramoorthy, E., Leonard, M., Mak, R., Liao, J., Fulzele, A., and Bennett, E.J. (2017). ZNF598 and RACK1 Regulate Mammalian Ribosome-Associated Quality Control Function by Mediating Regulatory 40S Ribosomal Ubiquitylation. Mol. Cell *65*, 751–760.e4.

Tao, X., and Gao, G. (2015). Tristetraprolin Recruits Eukaryotic Initiation Factor 4E2 To Repress Translation of AU-Rich Element-Containing mRNAs. Mol. Cell. Biol. *35*, 3921–3932.

Taylor, G.A., Carballo, E., Lee, D.M., Lai, W.S., Thompson, M.J., Patel, D.D., Schenkman, D.I., Gilkeson, G.S., Broxmeyer, H.E., Haynes, B.F., and Blackshear, P.J. (1996). A pathogenetic role for TNF alpha in the syndrome of cachexia, arthritis, and autoimmunity resulting from tristetraprolin (TTP) deficiency. Immunity *4*, 445–454.

Tiedje, C., Ronkina, N., Tehrani, M., Dhamija, S., Laass, K., Holtmann, H., Kotlyarov, A., and Gaestel, M. (2012). The p38/MK2-driven exchange between tristetraprolin and HuR regulates AU-rich element-dependent translation. PLoS Genet. *8*, e1002977.

Tiedje, C., Holtmann, H., and Gaestel, M. (2014). The role of mammalian MAPK signaling in regulation of cytokine mRNA stability and translation. J.I Interferon Cytokine Res. *34*, 220–232.

Tiedje, C., Diaz-Muñoz, M.D., Trulley, P., Ahlfors, H., Laaß, K., Blackshear, P.J., Turner, M., and Gaestel, M. (2016). The RNA-binding protein TTP is a global post-transcriptional regulator of feedback control in inflammation. Nucleic Acids Res. *44*, 7418–7440.

Winzen, R., Kracht, M., Ritter, B., Wilhelm, A., Chen, C.Y., Shyu, A.B., Müller, M., Gaestel, M., Resch, K., and Holtmann, H. (1999). The p38 MAP kinase pathway signals for cytokine-induced mRNA stabilization via MAP kinase-activated protein kinase 2 and an AU-rich region-targeted mechanism. EMBO J. *18*, 4969–4980.

Winzen, R., Thakur, B.K., Dittrich-Breiholz, O., Shah, M., Redich, N., Dhamija, S., Kracht, M., and Holtmann, H. (2007). Functional analysis of KSRP interaction with the AU-rich element of interleukin-8 and identification of inflammatory mRNA targets. Mol. Cell. Biol. *27*, 8388–8400.

Xue, Y., Zhou, Y., Wu, T., Zhu, T., Ji, X., Kwon, Y.S., Zhang, C., Yeo, G., Black, D.L., Sun, H., et al. (2009). Genome-wide analysis of PTB-RNA interactions reveals a strategy used by the general splicing repressor to modulate exon inclusion or skipping. Mol. Cell *36*, 996–1006.

Zhang, B., Kirov, S., and Snoddy, J. (2005). WebGestalt: an integrated system for exploring gene sets in various biological contexts. Nucleic Acids Res. *33*, W741-8.

Zuberek, J., Kubacka, D., Jablonowska, A., Jemielity, J., Stepinski, J., Sonenberg, N., and Darzynkiewicz, E. (2007). Weak binding affinity of human 4EHP for mRNA cap analogs. RNA *13*, 691–697.

STAR★METHODS

KEY RESOURCES TABLE

REAGENT or RESOURCE	SOURCE	IDENTIFIER
Antibodies		
Rabbit polyclonal anti-GIGYF1	Abcam	Cat # 121784; RRID: AB_11130603
Mouse monoclonal anti-GIGYF2 (A-12)	Santa Cruz Biotechnology	Cat # sc-393918
Rabbit polyclonal anti-ZNF598	Sigma Aldrich	Cat # HPA041760; RRID: AB_10794787
Rabbit polyclonal anti-TTP	Sigma Aldrich	Cat # T5327; RRID: AB_1841222
Rabbit monoclonal anti-MK2	Cell Signaling	Cat # 3042; RRID: AB_2141314
Mouse monoclonal anti-GFP (7.1)	Roche	Cat # 11814460001; RRID: AB_390913
Mouse monoclonal anti-FLAG (M2)	Sigma-Aldrich	Cat # F1804; RRID: AB_262044
Goat polyclonal anti-MCM6	Santa Cruz Biotechnology	Cat # sc-9843; RRID: AB_2142543
Rabbit monoclonal anti-PKM2 XP (D784A)	Cell Signaling	Cat # 4053; RRID: AB_1904096
Mouse monoclonal anti-Actin (C4)	Millipore	Cat # MAB1501; RRID: AB_2223041
Rabbit polyclonal anti-His-probe (H-15)	Santa Cruz Biotechnology	Cat # sc-803; RRID: AB_631655
Chemicals, Peptides, and Recombinant Proteins		
Doxycycline	Sigma-Aldrich	Cat # D3347
Interleukin-1 beta	Peprotech	Cat # 200-01B
Actinomycin D	Cayman Chemical	Cat # 50-76-0
GFP-Trap magnetic agarose	Chromotek	Cat # gtma_20
FLAG-M2 agarose	Sigma-Aldrich	Cat # A2220
RNase A	Thermo Fisher Scientific	Cat # EN0531
RNase I	Thermo Fisher Scientific	Cat # EN0602
RNase A (DNase-free)	Roche	Cat # 11119915001
DNase I	Ambion/Thermo Fisher Scientific	Cat # AM2238
SUPERase•IN RNase Inhibitor	Thermo Fisher Scientific	Cat # AM2696
RiboLock RNase Inhibitor	Thermo Fisher Scientific	Cat # EO0381
TRIzol® Reagent	Thermo Fisher Scientific	*Cat # 15596026*
T4-polynucleotide kinase (T4-PNK)	New England Biolabs, NEB	Cat # M0201
Bacterial 16S/23S rRNA	Roche	Cat #10206938001
Critical Commercial Assays		
RevertAid Reverse Transcriptase	Thermo Fisher Scientific	Cat # EP0441
SENSIFast SYBR Green No ROX qPCR mix	Bioline	BIO-98005
SENSIFast Probe No ROX qPCR mix	Bioline	BIO-86005
TaqMan Gene Expression assay for IL-8	Life Technologies	Cat #4331182
SYBR Green Quantitect assay for TNF (Hs_TNF_3_SG)	QIAGEN	Cat #QT01079561
NEBNext Ultra II directional kit	New England Biolabs, NEB	Cat # E7765
NEBNext Multiplex Oligos	New England Biolabs, NEB	Cat # E7335
NEBNext rRNA depletion kit	New England Biolabs, NEB	Cat # E6310
Deposited Data		
RAW and processed RNASeq data	This paper	GEO: GSE116126
PAR-CLIP data for ZNF598	Garzia et al., 2017	SRA: SRP095894
Experimental Models: Cell Lines		
Human osteosarcoma cells (U2OS)	ATCC	HTB-96; RRID:CVCL_0042
Human cervical cancer cells (HeLa)	ATCC	CCL-2; RRID:CVCL_0030
Human embryonic kidney cells (HEK293T)	ATCC	CRL-111268; RRID:CVCL_1926
See Table S4 for oligonucleotide information		

(*Continued on next page*)

Continued

REAGENT or RESOURCE	SOURCE	IDENTIFIER
Recombinant DNA		
pcDNA4/TO-GFP-GIGYF1	This paper	N/A
pcDNA4/TO-GFP-GIGYF2	This paper	N/A
pcDNA4/TO-GFP-ZNF598	This paper	N/A
pcDNA4/TO-GFP-TTP	This paper	N/A
pcDNA4/TO-FLAG-MKK6	This paper	N/A
pcDNA3-FLAG-ZNF598	Morita et al., 2012	N/A
pcDNA3.1-His-Strep-TTP	Winzen et al., 2007	N/A
pFLAG-4EHP	Okumura et al., 2007	Addgene Plasmid #17342
Software and Algorithms		
ImageJ version 1.50i	National Institute of Health (NIH), USA	https://imagej.nih.gov/ij
PRISM 7	GraphPad Software	https://www.graphpad.com/scientific-software/prism/
Galaxy Platform	Afgan et al., 2018	https://usegalaxy.org
DESeq2	Love et al., 2014	http://www.bioconductor.org/packages/release/bioc/html/DESeq2.html
CLAP pipeline		https://github.com/simras/CLAP
Pyicos	Althammer et al., 2011	https://bitbucket.org/regulatorygenomicsupf/pyicoteo/downloads/

CONTACT FOR REAGENT AND RESOURCE SHARING

Further information and requests for resources and reagents should be directed to and will be fulfilled by the Lead Contact, Simon Bekker-Jensen (email: sbj@sund.ku.dk).

EXPERIMENTAL MODEL AND SUBJECT DETAILS

The following cell lines were used in this study: Human osteosarcoma cells (U2OS), human embryonic kidney (HEK293T) cells and human cervical cancer (HeLa). They were cultured in DMEM medium supplemented with 10% fetal bovine serum, L-glutamine, penicillin and streptomycin. All cells were cultured at 37°C in a humidified incubator containing 5% CO_2. The cells were obtained from ATTC. Identifier can be found in the Key Resources Table.

METHOD DETAILS

Plasmids and siRNAs

Full length GIGYF1, GIGYF2, TTP and MKK6 cDNA was gateway cloned into the destination vectors pcDNA4/TO/GFP and pCDNA4/TO/FLAG. All mutations in GIGYF1 were introduced by site-directed mutagenesis using KOD DNA polymerase (Millipore) according to the manufacturer's instructions. pcDNA3-FLAG-ZNF598 (Morita et al., 2012) was a gift from Nahum Sonenberg (McGill University, Quebec, Canada) and subsequently sub-cloned into pcDNA4/TO/GFP using EcoRI and XhoI restriction sites. ZNF598 9P-9A was ordered as a synthetic gene (GeneArt) and sub-cloned into pcDNA4/TO/GFP-ZNF598 using EcoRI and XhoI restriction sites. Strep-tagged ZNF598 was generated by amplifying the cDNA using primers flanked by EcoRI and XbaI sites and subsequent exchange of the TTP coding sequence from pcDNA3.1-His-Strep-TTP (Winzen et al., 2007). pFLAG-4EHP was a gift from Dong-Er Zhang (Addgene plasmid #17342, (Okumura et al., 2007)). All constructs were verified by sequencing. All plasmid DNA transfections were done using FuGene 6 (Promega) according to the manufacturer's protocol. siRNA transfections were carried out using RNAiMAX (Life Technologies) following manufacturer's protocol. For siRNA target sequences (Eurofins) used in this study, see Table S4.

Cell culture and reagents

Human U2OS osteosarcoma cells, human embryonic kidney (HEK293T) cells and human cervical cancer (HeLa) cells were cultured in DMEM medium supplemented with 10% fetal bovine serum, L-glutamine, penicillin and streptomycin. All cells were cultured at 37°C in a humidified incubator containing 5% CO_2. To generate cell lines stably expressing GFP-GIGYF1, GFP-GIGYF2, GFP-ZNF598, GFP-TTP and FLAG-MKK6 under a doxycycline inducible promoter, cells were co-transfected

with pcDNA4/TO/GFP-GIGYF1/GIGYF2/ZNF598/TTP or pcDNA4/TO/FLAG-MKK6 and pcDNA6/TR (Life Technologies) in a 2:1 ratio and selected with Zeocin and Blasticidin (5 mg ml^{-1}) for 14 days. Individual clones were picked and analyzed for GFP-GIGYF1/GIGYF2/ZNF598/TTP or FLAG-MKK6 expression using western blot (WB) and immunofluorescence (IF) analyses. Chemicals used were Doxycycline (1 μg ml^{-1}), Interleukin-1 beta (2 ng ml^{-1}, Preprotech), Actinomycin D (10 μg ml^{-1}, Cayman Chemical) and MK2 inhibitor (MK2i) PF3644022 (10 μM, Sigma).

Immunochemical methods

GFP immunoprecipitations were performed with GFP-Trap agarose beads (Chromotek), FLAG pull-downs were performed using FLAG-M2 agarose beads (Sigma-Aldrich). All immunoprecipitations were carried out in low-salt EBC lysis buffer (150 mM NaCl; 50 mM Tris, pH 7.5; 1 mM EDTA; 0.5% NP40). For CLIP, GFP-Trap magnetic agarose beads were utilized (Chromotek). A final concentration of 50 μg/ml RNase A (Thermo Scientific) was used to test RNA-dependencies of protein-protein interactions. Indicated samples were incubated on ice for 20 minutes prior to immunoprecipitations. For RNA-IP experiments, U2OS cells were transiently transfected with pcDNA4/TO-GFP-ZNF598 or pEGFP-C1 (Clontech). 24h after transfection, the cells were lysed in low salt EBC buffer supplemented with RiboLock RNase Inhibitor (Thermo Scientific) and subjected to GFP-immunoprecipitation as described before. RNA was reclaimed from GFP-beads using TRIzol reagent (Thermo Scientific) according to the manufacturers protocol and analyzed by RT-qPCR. Antibodies used in this study included the following: anti-GIGYF1 (121784, Abcam, RRID: AB_11130603; WB 1:1000), anti-GIGYF2 (sc-393918, Santa Cruz Biotechnology; WB 1:500), anti-ZNF598 (HPA041760, Sigma Aldrich, RRID: AB_10794787; WB 1:5000), anti-TTP (T5327, Sigma Aldrich, RRID: AB_1841222; WB: 1:500), anti-MK2 (3042, Cell Signaling, RRID: AB_2141314; WB 1:1,000); anti-GFP (11814460001, Roche, RRID: AB_390913; WB 1:1,000), anti-FLAG-M2 (F1804, Sigma-Aldrich, RRID: AB_262044; WB 1:1,000, IF 1:500), anti-MCM6 (sc-9843, Santa Cruz, RRID: AB_2142543; WB 1:1,000), anti-PKM2 (4053, Cell Signaling, RRID: AB_1904096: WB 1:1,000), anti-His-Probe (H-15) (sc-803, Santa Cruz, RRID: AB_631655, WB 1:1,000), anti-Actin (C4) (MAB1501, Millipore, RRID: AB_2223041, WB 1:20,000).

CLIP

CLIP protocol was modified from (Tiedje et al., 2016). In short, U2OS cells transiently transfected with GFP-GIGYF1/2, GFP-RBM7, FLAG/GFP-ZNF598, FLAG-4EHP were washed washing with ice-cold PBS and irradiated with UV-C light (175 J m^{-2}, BS-02 irradiation chamber equipped with 254nm bulbs Gröbel Elektronik, Germany) and total cell extracts were obtained using lysis buffer (50 mM Tris/HCl [pH 8.0], 150 mM NaCl, 0.5% (v/v) Triton X-100 and 1 mM EDTA) and sonication (3 times for 20 s in ice). Lysates were cleared by centrifugation and incubated with with RNase A (For ZNF598: optimal concentration RNase A (Roche) = 1,88 × 10^{-3} units/ml and RNase I (Thermo Fischer Scientific) 1 unit/ml) and DNase I (20 units/ml, Ambion) for 3 min at 37˚C and cooled on ice for 5 min after adding urea (final concentration 0.5 M) and SUPERase IN RNase inhibitor (40 units/ml (Thermo Fischer Scientific). Immunoprecipitation of protein:RNA complexes was performed using FLAG-M2 beads or GFP-trap magnetic agarose beads. Samples were washed with lysis buffer plus 0.5 M Urea (2x) and high salt-urea wash buffer (50 mM Tris/HCl [pH 8.0], 1000 mM NaCl, 0.1% (v/v) Triton X-100 and 4M Urea) (3x) and PNK wash buffer (20 mM Tris–HCl [pH 7.4], 10 mM $MgCl_2$, 0.2% Tween-20) (2x. Samples were labeled with γ -^{32}P-ATP using T4-PNK (New England Biolabs). Then, protein:RNA complexes were resolved by electrophoresis (SDS-PAGE) and transferred to nitrocellulose membranes. Relative phosphorylation was assayed by radio-blotting.

Quantitative (q)PCR

Total RNA was purified from U2OS cells using TRIzol reagent (Invitrogen) according to the manufacturer's instructions. 350 ng of purified RNA was used in a reverse transcriptase reaction using random hexameric primers with RevertAid reverse transcriptase (Thermo Fisher) according to manufacturer's protocol. The generated cDNA was diluted 5-fold and used for quantification by qPCR (2,5ul diluted cDNA) using SensiFAST SYBR green (Bioline) or SensiFAST Probe (Bioline) mastermix according to the manufacturer's protocol. For detection of IL-8 mRNA, exon junction spanning TaqMan Gene Expression Assay probes (Life Technologies #4331182 and #4331182) were used. For detection of TNF mRNA, the Quantitect Hs_TNF_3_SG primerset (QIAGEN, QT01079561) was used. For all other trancripts DNA oligos were used for amplification. See Table S4 for oligonucleotide information. Relative RNA levels were calculated from ΔCt values compared to its respective control sample and normalized to GAPDH mRNA levels.

RNA-sequencing, mapping and differential gene expression analysis

rRNA-depleted total RNA-sequencing libraries from either siCTRL- or siZNF598-transfected cells were obtained by using the NEBNext Ultra II directional kit in combination with the NEBNext rRNA depletion kit (New England Biolabs, NEB, USA). 500 ng of total TRIzol-purified RNA was used as starting material for each sample and was processed according to manufacturer's instructions. For the final amplification of the libraries 6 cycles were run. For each condition, biological duplicate libraries were constructed. Prior to the 75 bp single end high output run on an Illumina NEXTSeq 500 (Illumina Inc., USA) system, libraries were analyzed and quantified with a Fragment Analyzer (Advanced Analytical Technologies, Inc., USA) and consequently multiplexed. The resulting RAW reads were demultiplexed and converted to the FASTQ format and groomed (FASTQ Groomer) before adaptor- and quality-trimming using "Trim Galore!." The reads were then mapped against human hg19 using RNA STAR (Galaxy version 2.6.0b-1). Trimming, quality control and mapping steps were conducted in the Galaxy platform (usegalaxy.org) (Afgan et al., 2018). To quantify expression counts

of reads overlapping by one or more base calls, the gene annotations made by the procedure described above were calculated using fjoin (Richardson, 2006) and a simple script to process the output of fjoin and associate counts to the gene IDs was also used. These count tables were loaded into R and analyzed using the DESeq2 R package (Love et al., 2014). Differential expression was calculated with DESeq2 standard settings. Heatmaps were generated following one of the default procedures described in the DESeq2 manual. Raw expression values were log-normalized (DESeq2 rlog function), each row was z-score normalized and genes were clustered by the default hierarchical clustering used in the heatmap.2 function.

PAR-CLIP

The two replicates of PAR-CLIP of ZNF598 (Garzia et al., 2017) were retrieved from Sequence Read Archive (SRA: SRP095894). Processing, mapping, normalization was done using the CLAP pipeline (Plass et al., 2017) and quantification of transcript binding affinity done as described in (Hansen et al., 2015). The datasets were processed with custom python scripts to trim low-quality base calls and remove 3′adapters. A read was called as a duplication artifact of PCR if there was another read in the set of unique reads with up to one base difference. For construction of the mapping index which was used in the mapping procedure of PAR-CLIP libraries, a reference assembly for human, hg19 was retrieved from the UCSC table browser. As PAR-CLIP reads contain T positions that are converted to C by the UV-radiation, this is accounted for in the substitution model in BWA-PSSM which assumes a conversion rate of 12.5% and other parameters that deviated from default were set to -n 0.04 -l 1024 -m 400 -P 0.5. Finally reads with a posterior probability of 0.99 or higher were called confidently mapped and those with a lower posterior probability multi-mappers.

For peak calling, normalization and quantification the Ensembl ver. 70 human annotation (Cunningham et al., 2015) was retrieved from the Ensembl ftp-site and processed such that only the longest protein coding transcript for each gene was selected. Using these gene models, respective annotations only containing exons, 3′UTRs and coding regions were made. To call and use only significant peaks, Pyicos (Althammer et al., 2011) was used with an annotation of exons, this method implements the modFDR (Xue et al., 2009). Following this procedure PAR-CLIP clusters of each library were normalized to the total library size by calculation of per base reads per million (RPM Equation 1).

$$e_i = \frac{10^6 c_i}{N} \quad (1)$$

Where c_i is the number of base calls at position i and N is the total number of base calls of the confidently mapped CLIP reads in each library. These quantities were summed along each mature transcript and divided by transcript length.

RNA electrophoretic mobility shift assay (REMSA)

Protein purification and REMSA was performed as described before (Tiedje et al., 2012). In brief, Strep-tagged TTP and ZNF598 were expressed in HEK293T cells and purified using Strep-affinity beads (IBA Technologies, Germany). Elution of proteins with desthiobiotin was followed by quantification in comparison to BSA standards and was followed by quantification of band intensities using the ImageJ software. According to these amounts the molarities of purified fusion proteins were calculated. For REMSAs, 400 fmol of a 5′FAM-labeled IL-8 RNA oligo (Integrated DNA Technologies, IDT, USA), corresponding to the minimal TTP binding site in the 3′UTR of IL-8 (Winzen et al., 2007), was incubated with the indicated protein amounts on ice for 20 minutes. To test for binding to ARE and polyA RNA stretches, 200 fmol of IRDye 700 and IRDye 800 5′-labeled RNAs were used. Then loading buffer was added to the samples that were consequently run on a pre-equilibrated 4% TBE polyacrylamide gel as described before (Tiedje et al., 2012). 5′FAM samples were analyzed on a Bio-Rad Chemidoc Imaging System (Bio-Rad Laboratories, USA) or were scanned with a LI-COR Odyssey CLx device (LI-COR, USA) in case of IRDye-labeled probes. Band intensities were determined using ImageJ software. For competition assays 4μg bacterial 16S and 23S rRNA was added per reaction (purchased from Roche #10206938001).

QUANTIFICATION AND STATISTICAL ANALYSIS

Statistical analyses were performed with GraphPad PRISM 7. Quantification of band intensities were carried out with the open source software ImageJ (version 1.50i). The number of technical or biological replicates that were applied are given in the corresponding figure legends. For relative mRNA level mean values ± standard deviations (SD) were calculated and significant changes were determined by unpaired t tests.

DATA AND SOFTWARE AVAILABILITY

The RNaseq and differential expression data was deposited at the Gene Expression Omnibus (GEO) archive under the accession number GSE116126.